



## Study on different power and cycling performance of crystalline $K_xMnO_2 \cdot nH_2O$ as cathode material for supercapacitors in $Li_2SO_4$ , $Na_2SO_4$ , and $K_2SO_4$ aqueous electrolytes

Jie Shao <sup>a</sup>, Xinyong Li <sup>a</sup>, Qunting Qu <sup>a,b,\*</sup>, Yuping Wu <sup>b,\*</sup>

<sup>a</sup> School of Energy & College of Chemistry, Chemical Engineering and Material Science, Soochow University, Suzhou, Jiangsu 215006, China

<sup>b</sup> Department of Chemistry & Shanghai Key Laboratory of Molecular Catalysis and Innovative Materials, Fudan University, Shanghai 200433, China

### HIGHLIGHTS

- $K_xMnO_2 \cdot nH_2O$  presents different electrochemical behaviors in three aqueous electrolytes.
- The reasons for the different electrochemical behaviors were elucidated.
- $K_xMnO_2 \cdot nH_2O$  displays a superior power and cycling performance in  $K_2SO_4$  electrolyte.

### ARTICLE INFO

#### Article history:

Received 10 May 2012

Received in revised form

7 August 2012

Accepted 14 September 2012

Available online 20 September 2012

#### Keywords:

Supercapacitor

Manganese dioxide

Power

Cycling performance

Electrolytes

### ABSTRACT

The charge/discharge, electrochemical impedance, cyclic voltammogram, and cycling behaviors of crystalline  $K_xMnO_2 \cdot nH_2O$  as cathode material for supercapacitors in  $Li_2SO_4$ ,  $Na_2SO_4$ , and  $K_2SO_4$  electrolytes were compared. The different power and cycling performance of  $K_xMnO_2 \cdot nH_2O$  during charge/discharge in the three electrolytes were elucidated by analyzing its composition and structure evolution. Compared with the  $Li_2SO_4$  and  $Na_2SO_4$  electrolytes, the highest ionic conductivity of  $K_2SO_4$  electrolyte, the fastest charge-transfer process and slightest structural evolution of  $K_xMnO_2 \cdot nH_2O$  during charge/discharge in the  $K_2SO_4$  electrolyte lead to a superior power and cycling behavior for supercapacitor application.

© 2012 Elsevier B.V. All rights reserved.

## 1. Introduction

Lithium ion batteries have become an indispensable part in our daily life ascribed to their wide applications as power sources of portable electronic devices. Correspondingly, a large quantity of lithium is being consumed every year. Especially, the imperative development of hybrid electric vehicles/electric vehicles based on lithium ion batteries will require hundreds or thousands of times the amount of lithium in portable devices [1,2]. Considering that the natural resources of lithium are limited, alternatives to lithium ion batteries are necessary in the long run. A feasible strategy is to explore novel energy storage systems using  $Na^+$  or  $K^+$  as working

ions [3–6]. Moreover,  $Na^+$  and  $K^+$  are more naturally abundant than  $Li^+$ , and their inorganic/organic salts are usually cheaper and more readily available than those based on  $Li^+$  [3]. Nonetheless, whether the electrochemical performance of energy storage systems based on  $Na^+$  or  $K^+$  working ions is superior to those based on  $Li^+$  is the key question that should be answered currently [7].

Supercapacitors are capable of working at much higher power density and possess a much longer cycling life than lithium ion batteries. Among the various high-energy electrode materials such as  $RuO_2$  [8],  $MnO_2$  [9–11],  $MoO_3$  [12], and  $V_2O_5$  [13,14] for supercapacitors,  $MnO_2$  is the most promising one for practical application due to its low cost, high faradic capacitance, and good cycling performance.  $MnO_2$  has been demonstrated to be capable of producing faradic capacitance using  $Na^+$  or  $K^+$  as well as  $Li^+$  as working ions [15]. In our previous work and other literature's report, manganese dioxides were found to present different

\* Corresponding authors.

E-mail addresses: [qtqu@suda.edu.cn](mailto:qtqu@suda.edu.cn) (Q. Qu), [wuyp@fudan.edu.cn](mailto:wuyp@fudan.edu.cn) (Y. Wu).

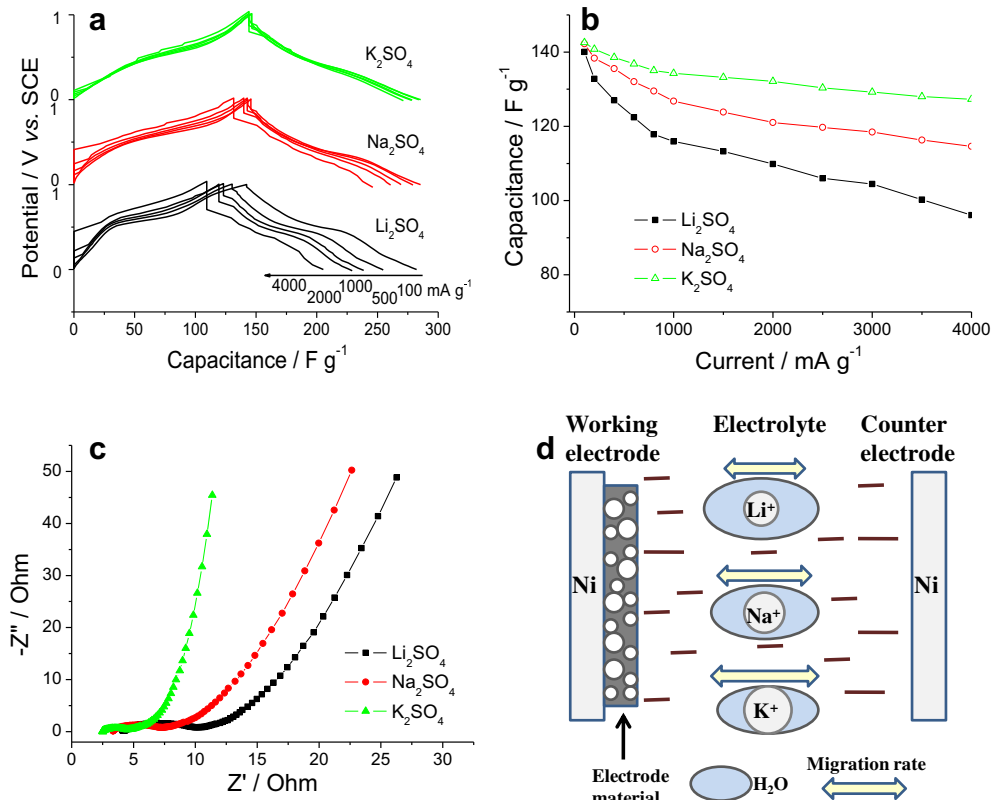


**Fig. 1.** (a) Galvanostatic charge/discharge curves of  $K_xMnO_2 \cdot nH_2O$  electrodes in  $Li_2SO_4$ ,  $Na_2SO_4$ , and  $K_2SO_4$  electrolytes at various current densities, (b) variation of discharge capacitance as the current density increases, (c) Nyquist plots of  $K_xMnO_2 \cdot nH_2O$  electrodes at the open-circuit potential, and (d) schematic illustration of the hydrated ionic radius and migration rate of three types of alkaline-metal cations.

capacitance and power ability in  $Li^+$ ,  $Na^+$ , and  $K^+$ -based electrolytes [15–18]. However, the reasons remain to be further understood and the effect of various electrolytes on the cycling ability of manganese dioxide also needs to be identified.

In this work, the different power and cycling performance of a crystalline birnessite- $MnO_2$ , namely  $K_xMnO_2 \cdot nH_2O$ , during charge/discharge in  $Li_2SO_4$ ,  $Na_2SO_4$ , and  $K_2SO_4$  aqueous electrolytes were elucidated by analyzing their electrochemical behaviors, and the corresponding composition and structural evolution. It was found that intercalation/deintercalation of  $Li^+$ ,  $Na^+$ , or  $K^+$  into/from the interlayer spacing of  $K_xMnO_2 \cdot nH_2O$  results in varying crystalline structure changes. Compared with the  $Li_2SO_4$  and  $Na_2SO_4$  electrolytes, the highest ionic conductivity of  $K_2SO_4$  electrolyte, the

fastest charge-transfer process and slightest structural evolution of  $K_xMnO_2 \cdot nH_2O$  during charge/discharge lead to the superior power and cycling performance in the  $K_2SO_4$  electrolyte.

## 2. Experimental

$K_xMnO_2$  precursor was prepared by ball-milling the mixture of  $K_2CO_3$  and  $MnO_2$  in a molar ratio of 1:2 for 12 h, followed by calcination at 550 °C for 8 h. The precursor was washed several times with water to remove residual  $K_2CO_3$  and then dried at 60 °C. Elemental analyses by energy dispersive X-ray (EDX, Philip XL30) and thermal gravimetric analysis (TGA, Perkin–Elmer TGA 7) for the as-prepared powder indicate that the primary composition of

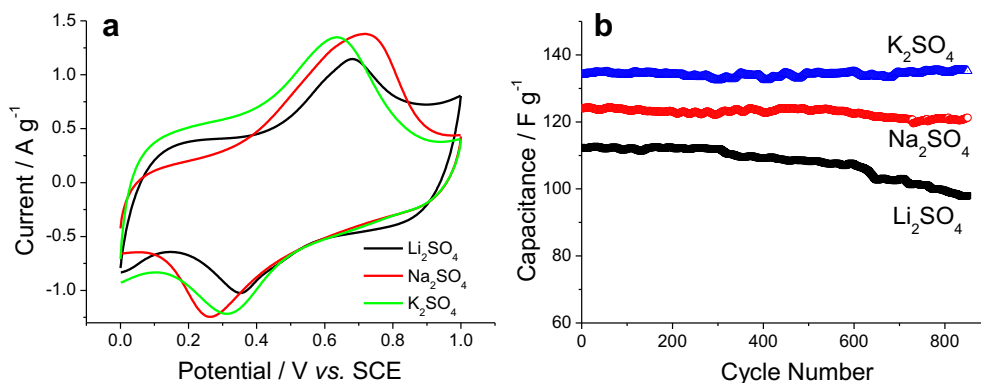


**Fig. 2.** (a) CV curves of  $K_xMnO_2 \cdot nH_2O$  electrodes in the three aqueous electrolytes at the scan rate of 5 mV s<sup>-1</sup>, and (b) capacitance change of  $K_xMnO_2 \cdot nH_2O$  electrodes during extended cycles.

the product is  $K_{0.3}MnO_2 \cdot 0.6H_2O$  [19]. The existence of  $H_2O$  results from the washing process during the preparation.

For electrochemical tests, the  $K_xMnO_2 \cdot nH_2O$  electrode was prepared by the following process. At first, a thin film composed of a mushy mixture of  $K_xMnO_2 \cdot nH_2O$ , acetylene black and poly(tetrafluoroethylene) (PTFE) in a weight ratio of 85:10:5 was prepared, and then punched into small disks with a diameter of 10 mm. These disks were pressed onto a Ni-grid at a pressure of 12 MPa and then dried at 70 °C for 5 h.  $Li_2SO_4$ ,  $Na_2SO_4$ , and  $K_2SO_4$  aqueous solutions with the concentration of 0.5 mol  $L^{-1}$  were used as electrolytes. Electrochemical tests of the  $K_xMnO_2 \cdot nH_2O$  electrodes were performed using a three-electrode cell, in which Ni-

grid and saturated calomel electrode (SCE) were used as the counter and the reference electrode, respectively. Cyclic voltammetric (CV) and galvanostatic charge/discharge tests of the  $K_xMnO_2 \cdot nH_2O$  electrode were performed in the potential range of 0–1.0 V vs. SCE. Electrochemical impedance spectra were recorded from  $10^5$  to 0.01 Hz, and the amplitude of the potential perturbation was 10 mV. X-ray diffraction (XRD, Rigaku D/MAX-IIA X-ray diffractometer) was used to investigate the structural changes of  $K_xMnO_2 \cdot nH_2O$  electrode at the end of charge and discharge. EDX was used to analyze the chemical composition of  $K_xMnO_2 \cdot nH_2O$  electrode during charge/discharge in  $Li_2SO_4$ ,  $Na_2SO_4$ , and  $K_2SO_4$  electrolytes.

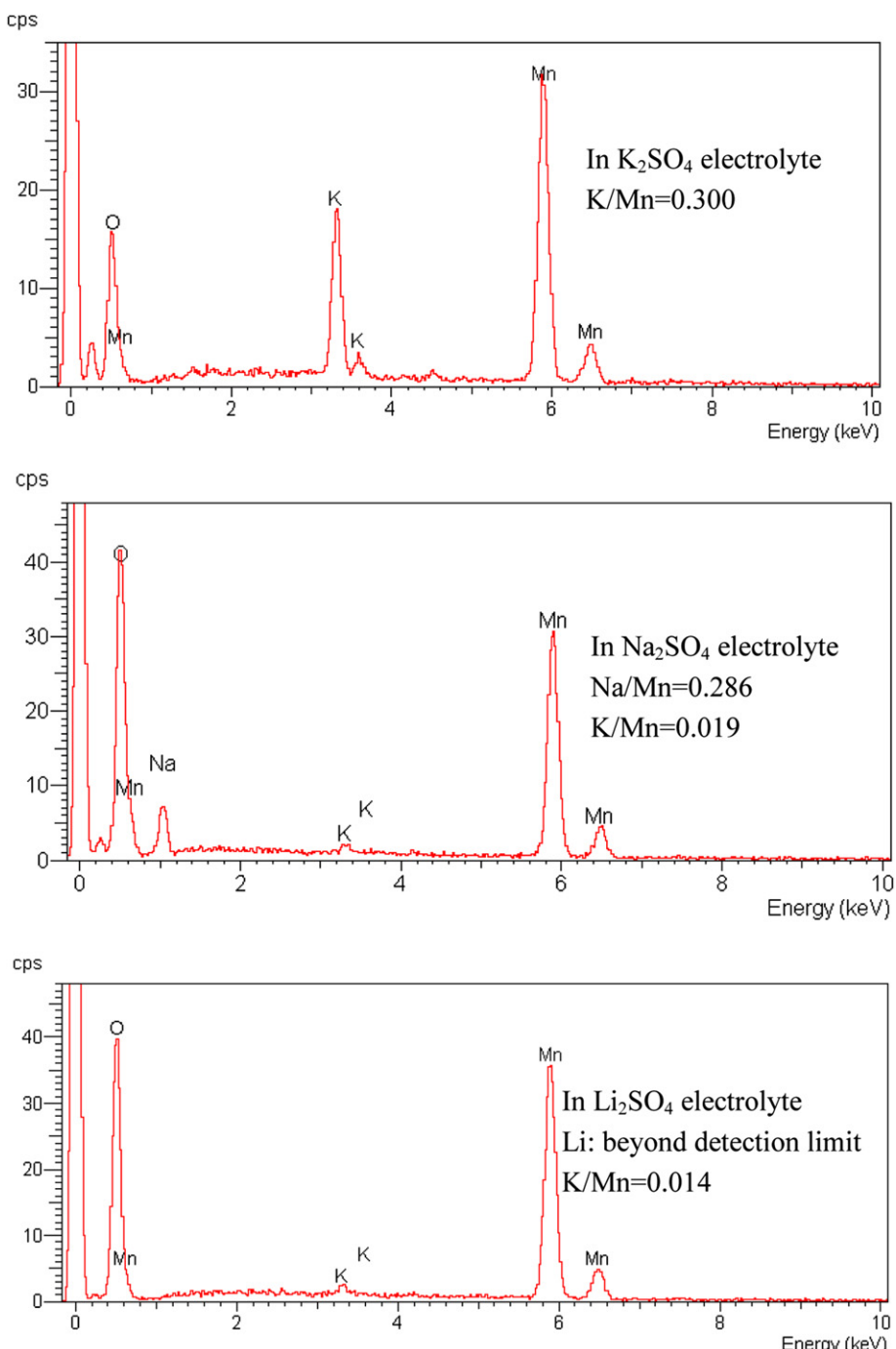


Fig. 3. EDX spectra and the corresponding chemical composition of  $K_xMnO_2 \cdot nH_2O$  electrodes after discharge in the three electrolytes.

### 3. Results and discussion

Previous work shows that the as-prepared  $K_xMnO_2 \cdot nH_2O$  materials are composed of aggregated particles with size ranging from 50 to 200 nm. A lamellar structure with thickness of less than 10 nm can be observed clearly for these particles [19]. A rather low BET surface area of  $4 \text{ m}^2 \text{ g}^{-1}$  is got due to the aggregation of these particles.

The galvanostatic charge/discharge curves of  $K_xMnO_2 \cdot nH_2O$  electrodes in  $Li_2SO_4$ ,  $Na_2SO_4$ , and  $K_2SO_4$  electrolytes at various current densities are shown in Fig. 1a. All the curves deviate from the ideal straight line, indicative of pseudocapacitive nature due to the  $Mn^{3+}/Mn^{4+}$  conversion. At a low current density of  $100 \text{ mA g}^{-1}$ ,  $K_xMnO_2 \cdot nH_2O$  presents similar discharge capacitance in the three electrolytes (about  $142 \text{ F g}^{-1}$ ). As the current density increases, the capacitance gradually decreases with different slopes (Fig. 1b). At the current density of  $4000 \text{ mA g}^{-1}$ ,  $K_xMnO_2 \cdot nH_2O$  maintains about 90% of its primary capacitance in  $K_2SO_4$  electrolyte, in sharp contrast to 68% of capacitance retention in  $Li_2SO_4$  electrolyte, suggesting a superior power ability of  $K_2SO_4$  electrolyte.

Electrochemical impedance spectroscopy was employed to investigate the electrode kinetics of  $K_xMnO_2 \cdot nH_2O$  in the three electrolytes. The open-circuit potentials of  $K_xMnO_2 \cdot nH_2O$  electrodes in  $Li_2SO_4$ ,  $Na_2SO_4$ , and  $K_2SO_4$  electrolytes are 0.34, 0.31, and 0.28 V vs. SCE, respectively. Nyquist plots of  $K_xMnO_2 \cdot nH_2O$  electrodes in the three electrolytes at the open-circuit potentials (Fig. 1c) are similar, consisting of a semicircle at mid-high frequency and a linear region at low frequency. The intercept on real axis at high frequency reflects the equivalent series resistance (ESR), which is related to the electrolyte resistance, intrinsic electrical resistance of grains, and the contact resistances of grain-to-grain and grain-to-current collector. The ESR values of  $K_xMnO_2 \cdot nH_2O$  electrodes in  $Li_2SO_4$ ,  $Na_2SO_4$ , and  $K_2SO_4$  electrolytes are 4.2, 3.3, and  $2.5 \Omega$ , respectively. The charge-transfer resistance ( $R_{ct}$ ) can be estimated from the diameters of semicircles on real axis. It can be seen that the charge-transfer process occurring on the electrode/electrolyte interface proceeds most readily in the  $K_2SO_4$  electrolyte. As for the linear region at low frequency, the more vertical the line is, the faster the capacitance is formed on the electrode surface. Among the three types of electrolytes,  $K_xMnO_2 \cdot nH_2O$  displays the most conspicuous capacitive feature in the  $K_2SO_4$  electrolyte. For the  $Na_2SO_4$  and  $Li_2SO_4$  electrolytes, the slope of the linear part is obviously smaller than that in  $K_2SO_4$ , suggesting that the electrode reaction tends to be under diffusion control. A schematic is shown in Fig. 1d to illustrate the different impedance behaviors of  $K_xMnO_2 \cdot nH_2O$  electrodes in the three aqueous electrolytes. The molar ionic conductivity of the three types of alkaline-metal ions in aqueous solutions ( $K$ :  $73.5 \text{ S cm}^2 \text{ mol}^{-1}$ ,  $Na$ :  $50.1 \text{ S cm}^2 \text{ mol}^{-1}$ ,  $Li$ :  $38.6 \text{ S cm}^2 \text{ mol}^{-1}$ ) [16], namely their migration rate, is supposed to account for the different electrolyte resistance and the corresponding ESR. Since the hydrated ionic radius of the three alkaline-metal ions are similar ( $K^+$ :  $3.31 \text{ \AA}$ ,  $Na^+$ :  $3.58 \text{ \AA}$ , and  $Li^+$ :  $3.82 \text{ \AA}$ ) [16], the different  $R_{ct}$  and capacitive features should be mainly affected by their different solvation interactions.  $K^+$  possesses the weakest solvation interaction with  $H_2O$  due to its smallest charge density, making it dehydrate readily in the interior of the porous electrode. As a result, the charge-transfer process occurs facilely and the double-layer capacitance is formed rapidly on the electrode/electrolyte interface. All the above impedance results explain the best power ability of  $K_xMnO_2 \cdot nH_2O$  in the  $K_2SO_4$  electrolyte.

CV curves of  $K_xMnO_2 \cdot nH_2O$  electrodes in the three aqueous electrolytes at the scan rate of  $5 \text{ mV s}^{-1}$  are presented in Fig. 2a. A couple of reversible redox peaks can be observed distinctly for all the three electrolytes, suggesting the faradic pseudocapacitive nature of  $K_xMnO_2 \cdot nH_2O$  material. Previous work on the crystalline structure

and chemical composition of  $K_xMnO_2 \cdot nH_2O$  during electrochemical cycles in  $K_2SO_4$  electrolyte indicates that this couple of redox peaks is concerned with the reversible intercalation/deintercalation of  $K^+$  into/from crystalline  $K_xMnO_2 \cdot nH_2O$  lattice [19–21]. In this work, the three types of electrolytes lead to slightly different potentials of these redox peaks. In addition, the redox peaks of  $K_xMnO_2 \cdot nH_2O$  electrodes are considerably more distinct than those of  $MnO_2$  reported in literatures, which can be ascribed to the high crystallinity of  $K_xMnO_2 \cdot nH_2O$  material. This phenomenon is consistent with that occurred on porous vanadium oxide during the redox transition, where intercalation/deintercalation of  $K^+$  can be enhanced by tuning the crystalline structure of vanadium oxide [22].

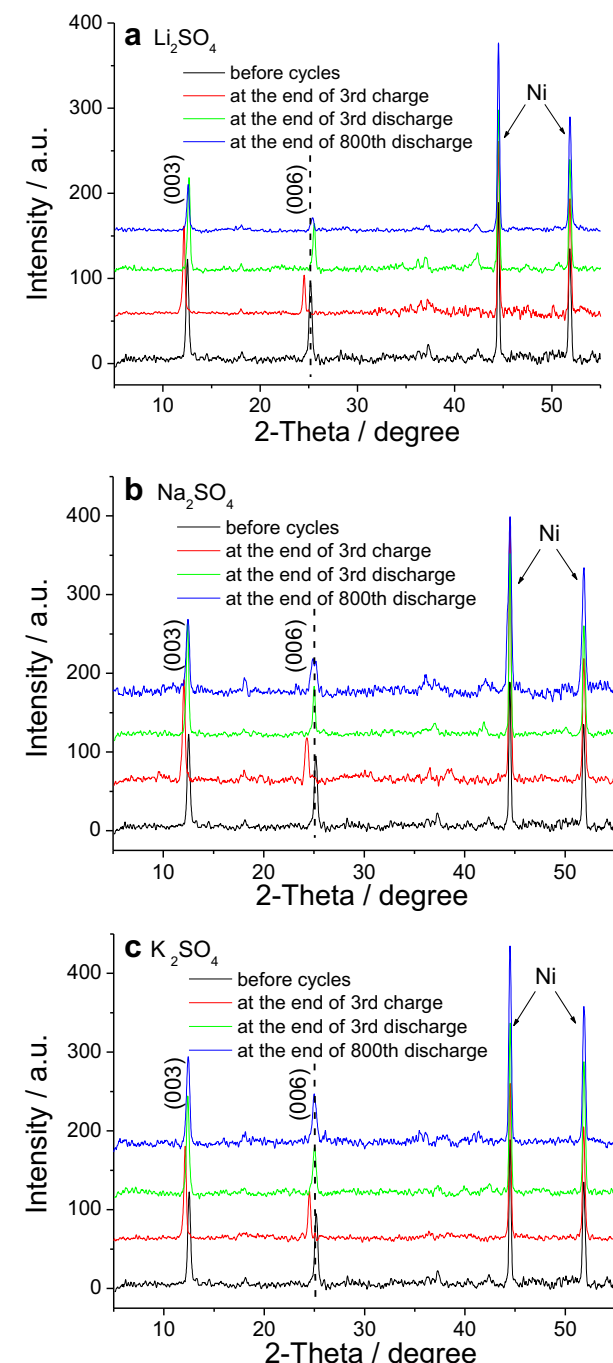


Fig. 4. Ex-XRD patterns of  $K_xMnO_2 \cdot nH_2O$  electrodes during charge/discharge at the current density of  $100 \text{ mA g}^{-1}$ .

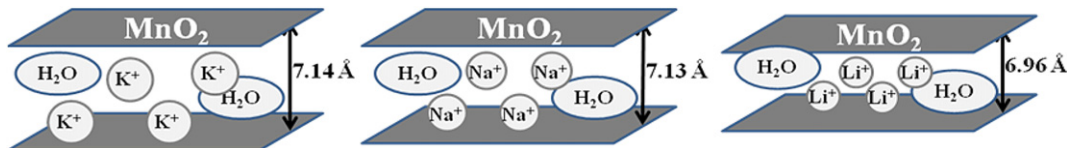


Fig. 5. The interlayer distance of  $K_xMnO_2 \cdot nH_2O$  material after the third discharge in the three electrolytes.

The capacitance change of  $K_xMnO_2 \cdot nH_2O$  electrode during extended cycles is shown in Fig. 2b. In the  $K_2SO_4$  electrolyte, no obvious capacitance loss is observed after 850 cycles. In contrast, the capacitance fades rapidly for the  $Li_2SO_4$  electrolyte with only 87% of capacitance retained. The different electrochemical behaviors of  $K_xMnO_2 \cdot nH_2O$  electrodes in the  $Li_2SO_4$ ,  $Na_2SO_4$ , and  $K_2SO_4$  electrolytes further prove that alkaline-metal ions participate in the electrode reaction.

Elemental analysis results obtained through EDX spectroscopy (Fig. 3) show a K/Mn atomic ratio of 0.300 in  $K_xMnO_2 \cdot nH_2O$  electrode after discharge (corresponding to intercalation of cations) in the  $K_2SO_4$  electrolyte. In contrast, after discharge in the  $Li_2SO_4$  and  $Na_2SO_4$  electrolytes, the energy peaks characteristic of K are very weak, and the corresponding K/Mn ratios (0.014 and 0.019) are much lower than that cycled in the  $K_2SO_4$  electrolyte. However, after discharge in the  $Na_2SO_4$  electrolyte, the energy peak characteristic of Na is strong, and the detected Na/Mn ratio (0.286) almost equals to the above K/Mn ratio of 0.300. Li cannot be detected through EDX because of the detection limit. These elemental analyses along with the above electrochemical characterizations validate that the major working ions of  $K_xMnO_2 \cdot nH_2O$  electrodes after the first cycle in the  $Li_2SO_4$ ,  $Na_2SO_4$ , and  $K_2SO_4$  electrolytes are  $Li^+$ ,  $Na^+$ , and  $K^+$ , respectively. It is noteworthy that the elemental analysis results are much different from those reported in literature [23]. Some researchers proposed that  $Na^+$  was not incorporated into the reduction reaction of  $MnO_2$  due to the absence of Na signal in the X-ray photoelectron spectra [23]. But in this work, the Na signal in the EDX spectra is very strong at the end of discharge. In our opinion,  $Na^+$  ions also participate in the redox reaction since  $K_xMnO_2 \cdot nH_2O$  manifests a very obvious intercalation/deintercalation reaction due to its high crystallinity.

Crystalline structure changes of  $K_xMnO_2 \cdot nH_2O$  electrodes after charge/discharge at the current density of 100  $mA\ g^{-1}$  were examined through XRD. As shown in Fig. 4, for all the three electrolytes, the interplanar spacing of  $K_xMnO_2 \cdot nH_2O$  increases slightly after the charge process (diffraction peaks at lower degree), and then decreases during the following discharge (diffraction peaks at higher degree). According to Bragg's law, the interplanar distance ( $d$ ) of  $K_xMnO_2 \cdot nH_2O$  can be calculated from XRD patterns. The  $d$  changes of (003) planes at the end of the third charge/discharge in the  $Li_2SO_4$ ,  $Na_2SO_4$ , and  $K_2SO_4$  electrolytes are calculated to be 0.29, 0.20, and 0.16  $\text{\AA}$ , respectively. Since  $K_xMnO_2 \cdot nH_2O$  electrode exhibits similar discharge capacitance in the three electrolytes at the current density of 100  $mA\ g^{-1}$ , its varying structural changes can be mainly ascribed to the different binding interactions of three types of alkaline-metal cations with the  $MnO_2$  framework. In addition, it is found that the interlayer distance decreases drastically after the discharge in the  $Li_2SO_4$  electrolyte. This should be due to the larger charge density of  $Li^+$  than those of  $Na^+$  and  $K^+$ , and its strong interaction with  $MnO_2$  framework makes the layered structure contract significantly (Fig. 5). The different structural evolution of  $K_xMnO_2 \cdot nH_2O$  in the three electrolytes further verifies the intercalation/deintercalation of different electrolyte cations. Furthermore, the above XRD analysis manifests one advantage of this work. In others' work, the intercalation/deintercalation process of  $Ca^{2+}$ ,  $Li^+$ ,  $Na^+$ , and  $K^+$  cannot be actually validated because of the low crystallinity of  $MnO_2$  materials [23,24].

The cycling performance of  $K_xMnO_2 \cdot nH_2O$  electrodes in the  $Li_2SO_4$ ,  $Na_2SO_4$ , and  $K_2SO_4$  electrolytes is also correlated to the different crystalline structure changes. The superior cycling behavior of  $K_xMnO_2 \cdot nH_2O$  in the  $K_2SO_4$  electrolyte (Fig. 2b) can be ascribed to its slightest structural expansion/contraction during charge/discharge, while the worst cycling behavior observed for the  $Li_2SO_4$  electrolyte corresponds to the significant interplanar distance changes. As we know, volumetric variations tend to result in gradual mechanical failure of electrode materials upon cycling and deteriorate the electrical contact among the constituent particles within the electrode [25]. For instance, significant volumetric changes of  $SnO_2$  [26] and  $Si$  [27] materials are detrimental to their long-term cycling behaviors. XRD patterns of  $K_xMnO_2 \cdot nH_2O$  electrodes after 800 cycles (Fig. 4) show that the crystallinity of  $K_xMnO_2 \cdot nH_2O$  in the  $Na_2SO_4$  and  $K_2SO_4$  electrolytes is maintained much better than that in the  $Li_2SO_4$  electrolyte. These results also suggest that drastic volume changes of  $K_xMnO_2 \cdot nH_2O$  during charge/discharge in the  $Li_2SO_4$  electrolyte result in significant structural degradation and poor cycling performance [28].

#### 4. Conclusion

The different electrochemical behaviors and the corresponding composition and structural evolution of crystalline  $K_xMnO_2 \cdot nH_2O$  during charge/discharge in the  $Li_2SO_4$ ,  $Na_2SO_4$ , and  $K_2SO_4$  electrolytes were investigated. Results indicate that intercalation/deintercalation of  $Li^+$ ,  $Na^+$ , and  $K^+$  into/from the interlayer spacing of  $K_xMnO_2 \cdot nH_2O$  occurs respectively in the three electrolytes. Compared with the  $Li_2SO_4$  and  $Na_2SO_4$  electrolytes, the highest ionic conductivity of the  $K_2SO_4$  electrolyte and fastest charge-transfer process of  $K_xMnO_2 \cdot nH_2O$  in the  $K_2SO_4$  electrolyte lead to the superior power ability. The cycling ability of  $K_xMnO_2 \cdot nH_2O$  was also found to be greatly influenced by the types of electrolytes.  $K_xMnO_2 \cdot nH_2O$  exhibits the best cycling behavior in the  $K_2SO_4$  electrolyte due to its slightest structural expansion/contraction degree during charge/discharge. This work not only reveals the superior electrochemical performance of  $MnO_2$ -based material by employing  $K^+$  as working ions, but also provides a new route for the exploration of novel energy storage systems substituting lithium ion batteries.

#### Acknowledgments

Financial support from National Natural Science Foundation of China (Nos. 21073046, 21073129 and 21203133) and Natural Science Foundation of Jiangsu Province (BK2012186) is greatly appreciated.

#### Appendix A. Supplementary data

Supplementary data related to this article can be found at <http://dx.doi.org/10.1016/j.jpowsour.2012.09.046>.

#### References

- [1] B.L. Ellis, W.R.M. Makahnouk, Y. Makimura, K. Toghill, L.F. Nazar, *Nat. Mater.* 6 (2007) 749.
- [2] C. Wadia, P. Albertus, V. Srinivasan, *J. Power Sources* 196 (2011) 1593.

- [3] V. Palomares, P. Serras, I. Villaluenga, K.B. Hueso, J. Carretero-Gonzalez, T. Rojo, *Energy Environ. Sci.* 5 (2012) 5884.
- [4] J.F. Whitacre, A. Tevar, S. Sharma, *Electrochem. Commun.* 12 (2010) 463.
- [5] B.L. Ellis, W.R.M. Makahnouk, W.N. Rowan-Weetaluktuk, D.H. Ryan, L.F. Nazar, *Chem. Mater.* 22 (2009) 1059.
- [6] Q.T. Qu, Y. Shi, S. Tian, Y.H. Chen, Y.P. Wu, R. Holze, *J. Power Sources* 194 (2009) 1222.
- [7] S.P. Ong, V.L. Chevrier, G. Hautier, A. Jain, C. Moore, S. Kim, X. Ma, G. Ceder, *Energy Environ. Sci.* 4 (2011) 3680.
- [8] R. Vellacheri, V.K. Pillai, S. Kurungot, *Nanoscale* 4 (2012) 890.
- [9] L. Mao, K. Zhang, H.S. Chan, J. Wu, *J. Mater. Chem.* 22 (2012) 1845.
- [10] Y.F. Yuan, Y.B. Pei, S.Y. Guo, J. Fang, J.L. Yang, *Mater. Lett.* 73 (2012) 194.
- [11] W. Tang, Y.Y. Hou, X.J. Wang, Y. Bai, Y.S. Zhu, H. Sun, Y.B. Yue, Y.P. Wu, K. Zhu, R. Holze, *J. Power Sources* 197 (2012) 330–333.
- [12] W. Tang, L.L. Liu, S. Tian, L. Li, Y.B. Yue, Y.P. Wu, K. Zhu, *Chem. Commun.* 47 (2011) 10058.
- [13] Q.T. Qu, Y. Shi, L.L. Li, W.L. Guo, Y.P. Wu, H.P. Zhang, S.Y. Guan, R. Holze, *Electrochem. Commun.* 11 (2009) 1325.
- [14] Q.T. Qu, Y.S. Zhu, X.W. Gao, Y.P. Wu, *Adv. Energy Mater.* 2 (2012) 950.
- [15] Q. Qu, P. Zhang, B. Wang, Y. Chen, S. Tian, Y. Wu, R. Holze, *J. Phys. Chem. C* 113 (2009) 14020.
- [16] R.N. Reddy, R.G. Reddy, *J. Power Sources* 124 (2003) 330.
- [17] H.Y. Lee, V. Manivannan, J.B. Goodenough, C.R. Acad. Sci. Paris-Ser. IIc 2 (1999) 565.
- [18] C. Ye, Z.M. Lin, S.Z. Hui, *J. Electrochem. Soc.* 152 (2005) A1272.
- [19] Q. Qu, L. Li, S. Tian, W. Guo, Y. Wu, R. Holze, *J. Power Sources* 195 (2010) 2789.
- [20] S.H. Kim, S.J. Kim, S.M. Oh, *Chem. Mater.* 11 (1999) 557.
- [21] H. Kanoh, W. Tang, Y. Makita, K. Ooi, *Langmuir* 13 (1997) 6845.
- [22] C.M. Huang, C.-C. Hu, K.-H. Chang, J.-M. Li, Y.-F. Li, *J. Electrochem. Soc.* 156 (2009) A667.
- [23] S.-L. Kuo, N.-L. Wu, *J. Electrochem. Soc.* 153 (2006) A1317.
- [24] C. Xu, H. Du, B. Li, F. Kang, Y. Zeng, *J. Electrochem. Soc.* 156 (2009) A73.
- [25] Y.-C. Hsieh, K.-T. Lee, Y.-P. Lin, N.-L. Wu, S.W. Donne, *J. Power Sources* 177 (2008) 660.
- [26] M.-S. Park, G.-X. Wang, Y.-M. Kang, D. Wexler, S.-X. Dou, H.-K. Liu, *Angew. Chem. Int. Ed.* 46 (2007) 750.
- [27] H.T. Nguyen, F. Yao, M.R. Zamfir, C. Biswas, K.P. So, Y.H. Lee, S.M. Kim, S.N. Cha, J.M. Kim, D. Pribat, *Adv. Energy Mater.* 1 (2011) 1154.
- [28] W. Wei, X. Cui, W. Chen, D.G. Ivey, *J. Power Sources* 186 (2009) 543.